Measuring, Modeling, and Decoupling of Saturation-Induced Saliencies in Carrier-Signal Injection-Based Sensorless AC Drives

Fernando Briz, Michael W. Degner, *Member, IEEE*, Alberto Diez, and Robert D. Lorenz, *Fellow, IEEE*

***Abstract*—The focus of this paper is the measuring, modeling, and decoupling of saturation-induced saliencies in carrier-signal injection-based sensorless control. First, techniques for the measurement of saturation-induced saliencies are presented. The goal of these measurements is to provide useful information on the position and magnitude of the various saturation-induced saliencies. Using the results from several different experimental measurements, models are developed explaining the source and behavior of the saturation-induced saliencies. The paper concludes by presenting methods for decoupling the effects caused by the parasitic saturation-induced saliencies, eliminating the errors that they cause in rotor position or flux angle estimation.**

***Index Terms*—Position estimation, self-sensing, sensorless control.**

I. Introduction

THE use of a high-frequency carrier signal superimposed on the fundamental excitation of an electric machine has established itself in recent years as a viable means of eliminating position sensors in ac drives for applications needing true zero-speed zero-frequency torque (and often also motion) control. The carrier signal interacts with spatial variations in the machine inductances or resistances (saliencies) producing a signal that can be used for the estimation of rotor position or flux angle [1]–[14].

Deterministically opening the slots above the rotor bars of an induction machine in a spatial harmonic pattern is one means to create a rotor position dependent variation in the rotor leakage inductance. This variation can be tracked by injecting a high-frequency carrier-signal excitation (voltage or current [7]) and a properly formed observer. In addition to this deterministic spatial variation of the rotor leakage inductance, other spatial inductance variations are often created by the saturation of the flux paths due to the fundamental excitation. Such secondary saliencies have been shown to cause estimation errors that can significantly reduce the overall control system performance [1]–[4], [9]–[11].

This type of secondary effect can be reduced (but not eliminated) by having a suitable minimal air gap above each of the rotor bars, which reduces the likelihood of saturation occurring in the rotor slot openings but not in any of the other flux paths. Alternatively, the estimation errors due to such secondary effects can be minimized by increasing the magnitude of the deterministic saliencies, thereby diminishing the relative contribution of the saturation-induced saliencies. However, significant practical limitations exist for the magnitude of the deterministic rotor position dependent saliency that can be created before it compromises the fundamental operation of the machine, e.g., decreased torque capability, increased ripple torque, etc. [9], [10].

This paper proposes a solution to this problem based on the measurement, modeling, and decoupling of the secondary saturation-induced saliency effects. The paper is organized as follows.

- First, techniques for the measurement of saturation-induced saliencies are presented. The goal of these measurements is to provide information on the position and magnitude of the various saturation-induced saliencies for a wide range of operating conditions. Of particular interest are the parasitic saliencies that can cause errors in the rotor position or flux angle estimate.
- Next, models that capture the behavior of saturation-induced saliencies are presented. For a motor with open rotor slots it will be shown that the saturation-induced saliencies detected by the carrier signal are created mainly by the stator leakage and air-gap flux.
- Finally, methods for decoupling these saliencies are presented. Implementing the decoupling method shows that the errors in the rotor position or flux angle estimate caused by the parasitic saturation-induced saliencies can be substantially reduced.

II. Flux, Position and Velocity Estimation Using Spatial Saliencies

To simplify the review of flux, position, and velocity estimation using spatial saliencies, the implementation based on

Paper IPCSD 01–046, presented at the 2000 Industry Applications Society Annual Meeting, Rome, Italy, October 8–12, and approved for publication in the IEEE TRANSACTIONS ON INDUSTRY APPLICATIONS by the Industrial Drives Committee of the IEEE Industry Applications Society. Manuscript submitted for review May 1, 2000 and released for publication July 16, 2001. This work was supported by the University of Oviedo, Ford Motor Company, and the Wisconsin Electric Machines and Power Electronics Consortium (WEMPEC), University of Wisconsin, Madison.

F. Briz and A. Diez are with the Department of Electrical, Computer and Systems Engineering, University of Oviedo, E-33204 Gijón, Spain (e-mail: fernando@isa.uniovi.es; alberto@isa.uniovi.es).

M. W. Degner is with the Scientific Research Laboratory, Ford Motor Company, Dearborn, MI 48121-2053 USA (e-mail: mdegner@ford.com).

R. D. Lorenz is with the Department of Mechanical Engineering and the Department of Electrical and Computer Engineering, University of Wisconsin, Madison, WI 53706 USA (e-mail: lorenz@engr.wisc.edu).

Publisher Item Identifier S 0093-9994(01)08617-0.

0093–9994/01$10.00 © 2001 IEEE

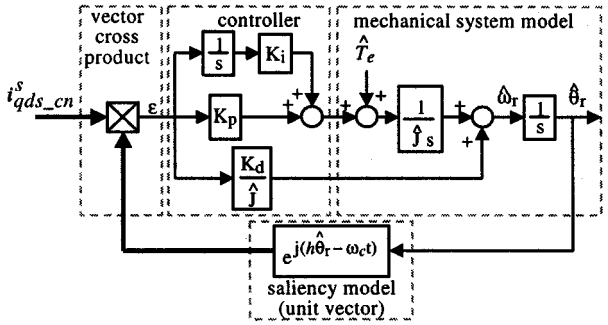

Fig. 1. Tracking observer for estimating rotor position in a machine with a single-rotor position-dependent saliency, implemented in a stationary reference frame.

having only a single sinusoidal spatial saliency present in the machine will be described. This saliency can be a result of either a deterministic, rotor position spatial modulation [1], [3], [4], [6]–[12] or saturation due to the rotor, stator, or air-gap flux [2], [5], [9], [10], [14]. Injection of a balanced polyphase carrier-signal voltage vector results in a carrier-signal current vector that can be used to estimate the position of the saliency using a vector cross product and a tracking observer, as shown in Fig. 1 [1], [2], [9].

When selecting the carrier-signal frequency, a low frequency is generally preferred because the sensing signal-to-noise ratio is improved. However, the lower limit is dictated primarily by the need for sufficient spectral separation from the fundamental frequency so that adequate estimation bandwidth is achievable. The carrier frequency is typically chosen to be in the range from a couple of hundred hertz to a kilohertz. For these carrier frequencies, the equivalent induction machine steady-state circuit is dominated by the stator transient impedance [1], [2], [9].

When the machine contains a saliency, the carrier signal current resulting from the injected voltage (1) contains both positive- and negative-sequence components (2). The positive-sequence carrier-signal current is proportional to the average stator transient inductance and contains no spatial information. The negative-sequence carrier-signal current is proportional to the differential stator transient inductance and contains spatial saliency position information in its phase [1], [2], [9]

$$v^s_{qds\_c} = V_c e^{j\omega ct} \tag{1}$$

$$i^s_{qds\_c} = i^s_{qds\_cp} + i^s_{qds\_cn} = -jI_{cp}e^{j\omega ct} + jI_{cn}e^{j(h\theta e - \omega ct)} \tag{2}$$

where θ_e is the angular position of the saliency in electrical radians, h is the harmonic number of the saliency, ω_c is the carrier frequency in radians per second, $L_{\sigma qs}$, $L_{\sigma ds}$ are the q- and d-axes stator transient inductances in the saliency synchronous reference frame, $\Sigma L_{\sigma s} = (L_{\sigma qs} + L_{\sigma ds})/2$ is the average stator transient inductance, $\Delta L_{\sigma s} = (L_{\sigma qs} - L_{\sigma ds})/2$ is the differential stator transient inductance, $I_{cp} = (V_c/\omega_c)(\Sigma L_{\sigma s}/\Sigma L_{\sigma s^2} - \Delta L_{\sigma s^2})$ is the magnitude of the positive sequence carrier signal current, and $I_{cn} = (V_c/\omega_c)(\Delta L_{\sigma s}/\Sigma L_{\sigma s^2} - \Delta L_{\sigma s^2})$ is the magnitude of the negative sequence carrier signal current.

TABLE I
INDUCTION MOTORS PARAMETERS

	MOTOR 1†	MOTOR 2
Stator Slots	24	24
Rotor Slots	30	30
R'_S	8.4	–
$L_{\sigma s}$	31 mH	–
Power Rating	0.75 kW	1.5 kW
Poles	4	2

† Skewed, closed rotor slots (prior to modification)

Fig. 2. Rotor of a 0.75-kW induction machine used for the test.

When carrier-signal excitation is used for sensorless control, the overall stator current consists of the fundamental current and the positive- and negative-sequence carrier-signal currents. The separation of these components is necessary for both the fundamental current regulator operation and the extraction of the spatial information from the negative-sequence carrier signal. Though different filter designs are possible, the use of synchronous frame bandstop filters has been shown to provide excellent results [6], [10], [12].

III. INFLUENCE OF SATURATION-INDUCED SALIENCIES ON THE ESTIMATED POSITION

To analyze the influence of saturation-induced saliencies on the estimated rotor position, experimental tests were conducted on a 0.75-kW induction machine with closed rotor slots and the parameters shown in Table I, motor 1 (prior to its modification). A quasi-sinusoidal rotor-dependent saliency with period equal to the pole pitch was introduced by opening the rotor slots, Fig. 2. Fig. 3(a) shows a schematic representation of the modification, while Fig. 3(b) shows the corresponding slots openings. A switching frequency in the inverter of 15 kHz, which is equal to the sampling frequency of the controller, was used. The algorithms were implemented on a TMS320C30 digital signal processor (DSP) running at 25 MHz. A carrier-signal magnitude of $V_c = 15$ V and frequency of $\omega_c = 537$ Hz were used.

Fig. 4 shows the fast Fourier transform (FFT) of the stator current complex vector when the motor is excited by a carrier voltage with the rotor locked and no fundamental excitation [15]. The spectrum is seen to consist of the positive- and negative-sequence carrier-signal current components, with magni-

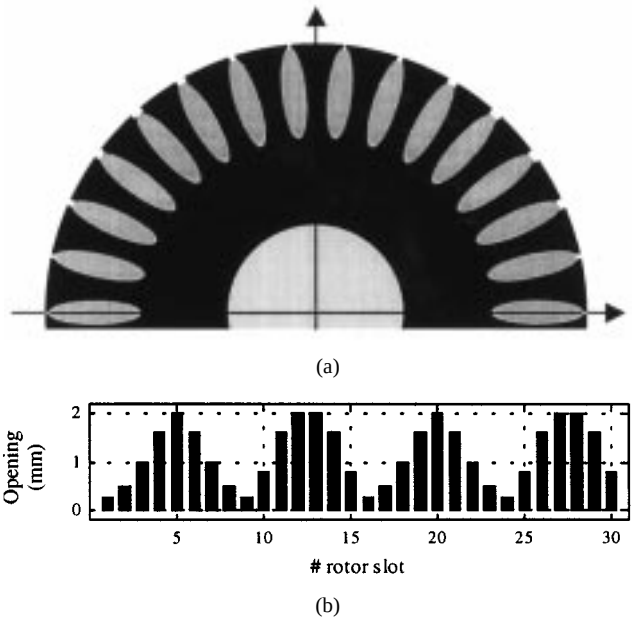

Fig. 3. Modification introduced in the rotor. (a) Schematic representation over a two-pole-pitch angle. (b) Openings introduced in the rotor slots. Slot openings of 0.25, 0.5, 0.8, 1.0, 1.6, and 2.0 mm, all openings have a constant depth of approximately 0.5 mm.

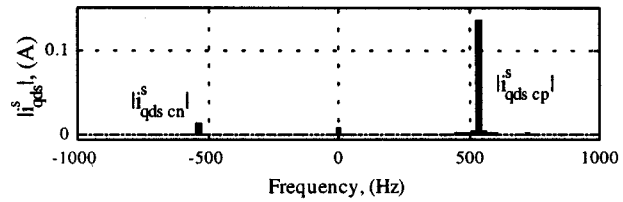

Fig. 4. FFT of the stator current complex vector in the stationary reference frame, with $\omega_r = 0$ Hz and no fundamental current. $V_c = 15$ V, $\omega_c = 537$ Hz.

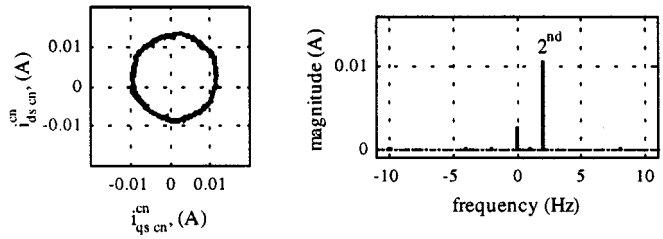

Fig. 5. Trajectory and FFT of the negative-sequence carrier-signal current complex vector in the negative-sequence carrier-signal reference frame at constant rotor speed, with $\omega_r = 1$ Hz (30 r/min) and no fundamental current.

tudes relative to the rated fundamental current of less than 4.5% and 0.3%, respectively.

The trajectory and FFT of the negative-sequence carrier-signal current when the motor rotates at constant speed with no fundamental excitation in the machine can be seen in Fig. 5. It can be seen that the rotor-dependent saliency creates mainly a harmonic that rotates at twice the electrical rotor speed (four times the rotor mechanical speed for a four-pole machine). From this figure, it is also seen that the negative-sequence current contains a dc component in the negative-sequence reference frame, i.e., which does not move

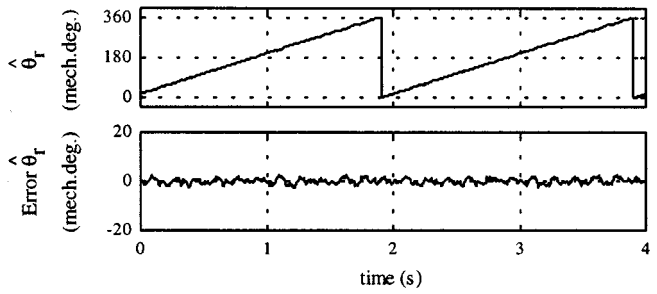

Fig. 6. Estimated rotor position and estimated rotor position error, with $\omega_r = 1$ Hz (30 /min) and no fundamental current.

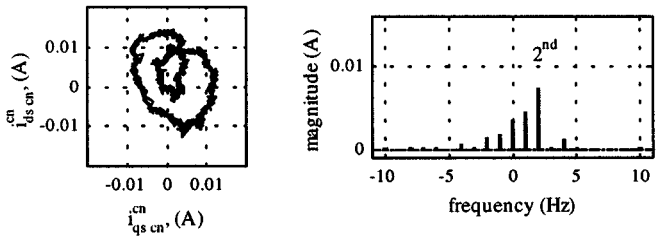

Fig. 7. Trajectory and FFT of the negative-sequence carrier-signal current complex vector in the negative-sequence reference carrier-signal frame at constant rotor speed, with $\omega_e = -1$ Hz, $\omega_r = 1$ Hz (30 r/min), and rated fundamental current.

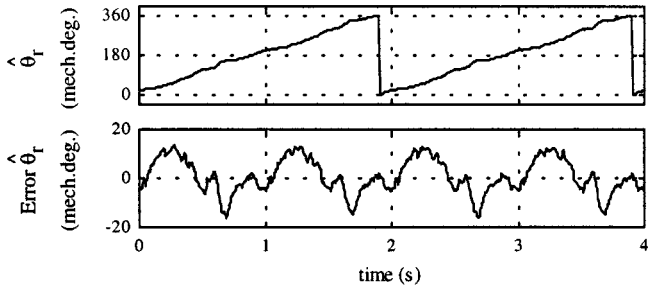

Fig. 8. Estimated rotor position and estimated rotor position error, with $\omega_e = -1$ Hz, $\omega_r = 1$ Hz (30 r/min), and rated fundamental current.

with the rotor. This component corresponds to a stationary saliency, since it is fixed relative to the stator. Different gains in the current sensors and/or asymmetries in the machine are the most likely causes of such a stationary saliency [6], [10]. Fig. 6 shows the estimated position using the tracking observer from Fig. 1, after the stationary saliency has been decoupled [6], [10].

When fundamental current exists, in addition to the rotor-dependent saliency, saturation-induced saliencies are often present. Figs. 7 and 8 show the negative-sequence carrier current trajectory and the corresponding FFT, and the estimated rotor position, respectively, for the case of operation at rated current-rated slip. Figs. 9 and 10 show the results for the case of a no-load, rated flux condition. The presence of the fundamental current is seen to create additional harmonics in the negative-sequence current. The adverse effect of the saturation-induced saliencies on the estimated position due to the fundamental current is evident when comparing Figs. 8 and

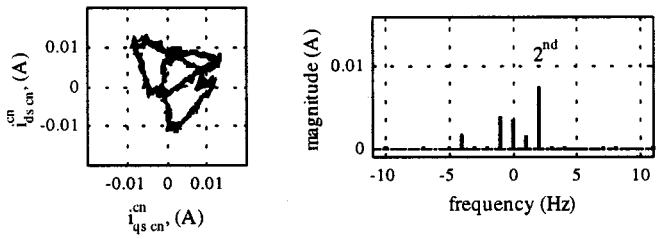

Fig. 9. Trajectory and FFT of the negative-sequence carrier-signal current complex vector in the negative-sequence reference carrier-signal frame at constant rotor speed, with $\omega_e = 1$ Hz, $\omega_r = 1$ Hz (30 r/min), and rated flux.

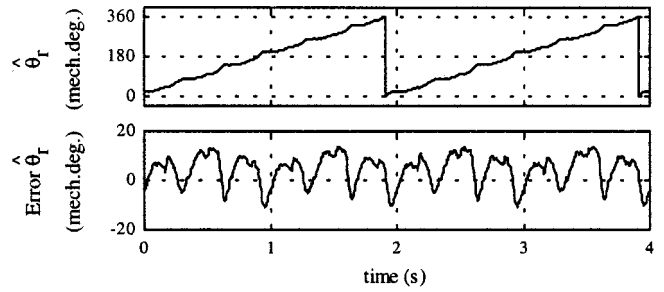

Fig. 10. Estimated rotor position and estimated rotor position error, with $\omega_e = 1$ Hz, $\omega_r = 1$ Hz (30 r/min), and rated flux.

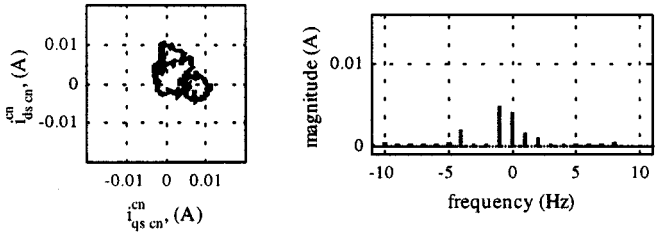

Fig. 11. Trajectory and FFT of the negative-sequence carrier-signal current complex vector in the negative-sequence carrier-signal reference frame with the rotor removed, for rated fundamental current, $\omega_e = 1$ Hz.

10 with Fig. 6, which was the case with no fundamental current excitation.

IV. Measuring and Modeling Saturation-Induced Saliencies

The influence of saturation-induced saliencies on the position estimation has been addressed by different researchers [1]–[4], [8]–[11], [13]. This analysis has typically been limited to the study of the harmonic at $2 \cdot \omega_e$, assuming that the saturation-induced saliency will form a sinusoidal spatial distribution with its period equal to the pole pitch [11], [13].

Experimental results reveal that additional, nonnegligible harmonics are present. Furthermore, it is difficult to distinguish between saturation-induced saliencies caused by the air-gap flux, stator leakage flux, or rotor leakage flux.

From the experimental results presented in the previous section, it is interesting to note the $\pm\omega_e$ harmonics in the negative-sequence carrier current when the fundamental excitation is present. Any saliency that is periodic over a pole pitch and is rotating at ω_e should give rise to harmonics with an order $\pm 2h\omega_e$, with $h = 1, 2, 3, \ldots$. The $\pm\omega_e$ harmonics do not follow this relationship. The $\pm\omega_e$ harmonics might be explained as the consequence of physical asymmetries in the stator windings. Another potential explanation is a dynamic eccentricity of the rotor that might give rise to $\pm\omega_r$ harmonics, which for the case of no-load condition would rotate at the same speed as the $\pm\omega_e$ harmonics. However, this would not be true for loaded conditions. Nevertheless, these physical differences should be attenuated in machines with more than two poles, since their period would not match the stator windings fundamental period and would not be expected to create large saliencies.

Another potential explanation for these harmonics could be the carrier signal being able to "see"/detect not only a saturation-induced saliency, but also its polarity. In essence, the carrier signal is able to distinguish between a north and a south pole of the fundamental flux (either leakage or magnetizing flux) due to the nonlinear interaction of the fundamental flux and the carrier-signal flux due to saturation. This issue is further discussed in the next section.

It should also be noted that for all the machines tested during this research, the $\pm\omega_e$ harmonics were only present when fundamental excitation existed, which points toward the fundamental flux rather than physical differences as the most likely source.

A. Influence of the Stator Leakage Flux

To separately investigate the influence of the stator leakage flux, experiments were carried out with the rotor removed from the stator. When a carrier signal is injected under this condition, any saliency observed may possibly be attributed to the saturation due to the stator leakage flux, since no air-gap or rotor flux exists. Fig. 11 shows the measured negative sequence carrier signal current and the corresponding FFT when fundamental current is injected with the rotor removed. It is seen that even though no air-gap flux exists, a noticeable saturation-induced saliency was created. It is also interesting to compare the FFT in Fig. 11 with the one in Fig. 9. Except for the 2nd harmonic present in Fig. 9, which is due to the deterministic spatial variation of the rotor slot openings and is therefore not present in Fig. 11, the remaining harmonics are strikingly similar. This data strongly supports the hypothesis that saturation due to the stator leakage flux could also be a source of saturation-induced saliencies when the rotor is present. A stator leakage flux contribution to saturation-induced saliencies was also observed previously in [13].

It is also interesting to notice that the $\pm\omega_e$ harmonics are present in Fig. 11, which eliminates any rotor eccentricity as a potential source for these harmonics. It has been claimed that the $\pm\omega_e$ harmonics are the results of a north/south-pole effect associated with the air-gap flux [14]. The fact that the rotor is not present in this experiment contradicts that explanation. None of the experiments carried out during this research, including those with the rotor present, suggest that the air-gap flux gives rise to this behavior. Consequently, a north/south-pole effect due to the stator leakage flux seems to the most likely origin. Nevertheless, this hypothesis is still unverified.

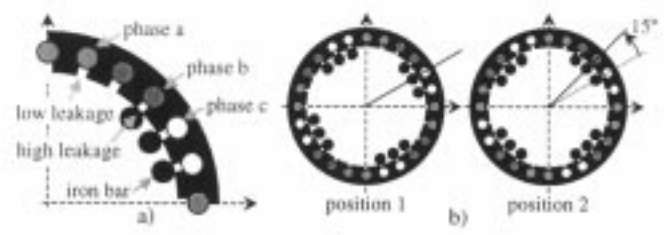

Fig. 12. (a) Variation of the stator leakage inductance over a pole pitch (four-pole machine) by closing the stator slot using ferromagnetic material (iron bars). (b) Rotation of the saliency between two consecutive positions.

B. Modulation of the Stator Leakage Inductance

Additional experiments were carried out with the rotor removed in order to verify how saliencies interact with the stator windings and which harmonics should actually be expected in the negative-sequence current. With the rotor removed, spatial modulation of the stator leakage inductance can easily be achieved by placing ferromagnetic material (iron bars) over some of the stator slots, as shown in Fig. 12(a).

By covering some of the stator slots with iron bars, high-leakage flux paths (high stator leakage inductance) are created. Fig. 12(b) shows one possible placement of the iron bars for the case of the four-pole machine whose parameters are listed in Table I, motor 1. For this case, a saliency period equal to six stator slots, i.e., one pole pitch was chosen. This corresponds to the 2nd spatial harmonic with a period equal to two pole pitches used as the reference (4th spatial harmonic when 360 mechanical degrees is used as the reference). A symmetric pattern of three closed and three open stator slots was chosen. This creates a symmetric square-wave spatial modulation of the stator leakage permeance, which should yield mostly odd multiples of the fundamental harmonic of the saliency. The saliency can easily be rotated by simply moving the iron bars, as shown in Fig. 12(b). Of course, only discrete positions of the saliency can be obtained with this method, since the rotation step is one stator slot, corresponding to 15 mechanical degrees for this case.

Despite the simplicity of this experiment, some interesting conclusions can be reached. Fig. 13–2(a) and (b) shows the negative-sequence carrier current created when the two, one pole pitch patterns shown in Fig. 13-1(a) and (b) were used.

The first case, shown in Fig. 13-1(a), is a symmetric square-wave spatial modulation (essentially odd harmonics). The resulting negative-sequence carrier current trajectory as the saliency is rotated is shown Fig. 13-2(a). The trajectory consists of only six points since the saliency created by the iron bars repeats after moving six stator slots. The FFT of the negative-sequence carrier current is shown in Fig. 13-3(a). When the saliency is rotated two pole pitches (180 mechanical degrees, equivalent to 360 electrical degrees for a four-pole machine), the negative-sequence carrier-signal current in Fig. 13-2(a) rotates two complete turns. Using the electrical angle of the saliency as the base angle, the negative-sequence carrier-signal current is mostly a 2nd harmonic, as shown in Fig. 13-3(a), with a stationary saliency. The fact that no noticeable additional harmonics exist is due to the way that most conventional polyphase machines are wound, i.e., the

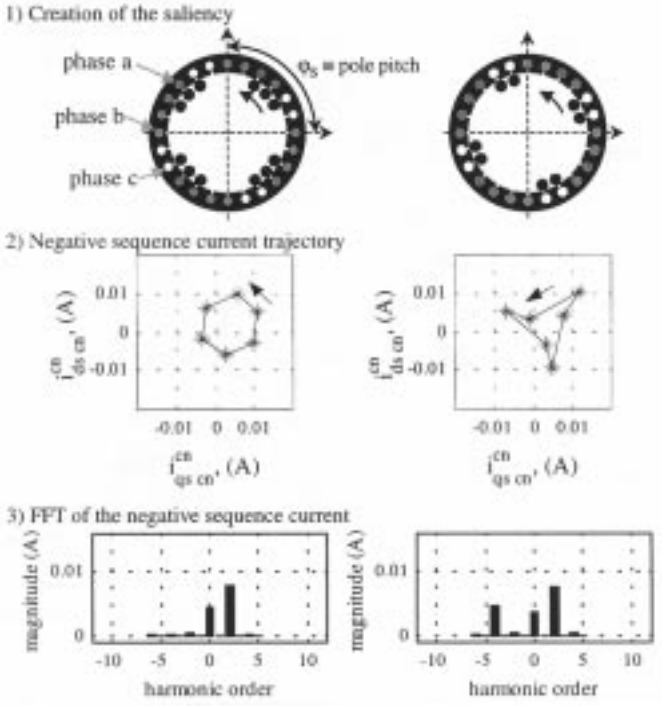

(a) (b)

Fig. 13. Creation of a spatial modulation in the stator leakage inductance using two different patterns. Both negative-sequence currents and FFT shown in a negative-sequence carrier reference frame. (a) Saliency consisting of a 2nd spatial harmonic fundamental and odd multiples. (b) Saliency consisting of a 2nd spatial harmonic fundamental and both odd and even multiples.

stator windings are designed to accentuate the fundamental spatial components and to attenuate higher spatial harmonics. Thus, a symmetric square-wave permeance modulation results in an almost sinusoidal inductance modulation when seen by the stator windings [9].

For the second case, an asymmetric square wave, one pole pitch pattern was used (four open, two closed), as shown in Fig. 13-1(b). The asymmetry results in both odd and even permeance harmonics. Fig. 13-2(b) shows the negative-sequence carrier current and Fig. 13-3(b) the corresponding FFT. The even harmonics in the saliency interact with the stator windings resulting in additional harmonics in the negative-sequence carrier current, whose trajectory is no longer a circular pattern. From Fig. 13-3(b), it is seen that the -4th harmonic shows up with a significant magnitude. The -4th harmonic is also commonly found for the case of saturation-induced saliencies, as seen in Figs. 7, 9, and 11.

To further explain the origin of the -4th harmonic, an additional experiment was performed. A two-pole machine was used (Table I, motor 2). Fig. 14-2(a) and (b) shows the negative-sequence carrier-signal current and Fig. 14-3(a) and (b) the corresponding FFT for the two different spatial modulations in the stator leakage inductance of Fig. 14-1(a) and (b).

It is noted that, for the two cases, the saliency was rotated in the positive (counterclockwise) direction. For the first case, Fig. 14(a), a symmetric square-wave modulation with its fundamental period equal to the pole pitch (2nd spatial harmonic) was created. The negative-sequence carrier current is seen to consist of mostly a 2nd harmonic, in addition to a stationary saliency.

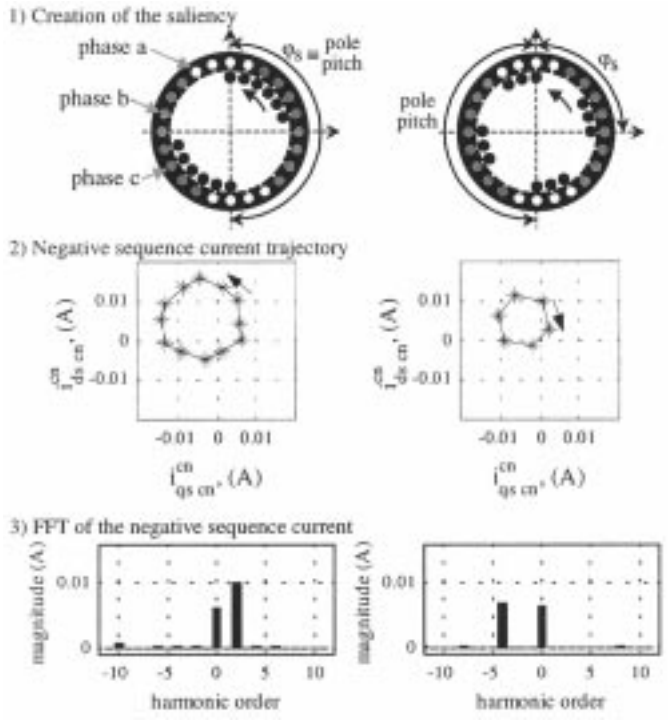

(a) (b)

Fig. 14. Creation of a symmetric square-wave spatial modulation in the stator leakage inductance with its fundamental period equal to (a) the pole pitch (2nd spatial harmonic and odd multiples), and (b) half of the pole pitch (4th spatial harmonic and odd multiples). Both negative-sequence currents and FFT shown in a negative-sequence carrier reference frame.

For the second case, Fig. 14(b), a symmetric square wave modulation with its fundamental period equal to half of the pole pitch (4th spatial harmonic) was created. The negative sequence carrier again describes a circular trajectory, but now consisting of mostly a $-$4th harmonic, i.e., it rotates backward. This demonstrates that a spatial modulation with its period equal to half of the pole pitch, intrinsically creates an inductance variation that rotates backward relative to the direction that the saliency rotates.

Additional experiments with different periods in the created saliency were performed (but not included in this paper due to space constraints). The following general conclusion was reached. With φ_s being the harmonic saliency period in mechanical degrees (3), only when (4) is satisfied will it couple with the stator winding and result in a negative-sequence current

$$\varphi_s = \frac{2\pi}{h_{sp}} \tag{3}$$

$$h_{sp} = n \cdot p = 1, 2, 4, 5, 7, 8, 10, \ldots \tag{4}$$

where p is the number of poles and h_{sp} is the saliency harmonic order relative to 360 mechanical degrees.

The resulting negative-sequence current for each saliency harmonic rotates at a speed (in electrical units) in the negative-sequence reference frame equal to $n \cdot p$ times the mechanical speed ($2 \cdot n$ times the electrical speed) of the saliency. In addition, it rotates in the same direction as the saliency when n is equal to 1, 4, 7, 10 ... (i.e., $n = 1+$ integer multiples of 3), and in the opposite direction as the saliency when n is equal to 2, 5, 8, 11 ... (i.e., $n = 2+$ integer multiples of 3). The case of n equal to integer multiples of three, i.e., $n = 3, 6, 9 \ldots$ does not result in any negative-sequence current.

C. Modeling of Saturation-Induced Saliencies

The development of a theoretical model for the relationship between the saliencies in a machine and the resulting negative-sequence carrier-signal current can be divided into two distinct steps.

1) The first is calculation of the required permeance spatial distribution that results in it coupling with the machine windings to produce an inductance variation.
2) The second is development of the relation between the speed of rotation of the source of the permeance variation, i.e., a component of the flux or the rotor position, to the speed at which the permeance variation itself rotates and then ultimately to the speed of rotation of the resulting negative-sequence carrier-signal current.

This section briefly discusses the development of a model using these steps and summarizes some of the general conclusions that result from such a model.

The mutual inductance between two windings, x and y, can be modeled as shown in (4) [10], [16]

$$L_{xy} = \frac{\lambda_{xy}}{i_y} = \int_0^{2\pi} P(\theta_s, \theta_r, \theta_e) N_x(\theta_s) N_y(\theta_s)\, d\theta_s \tag{5}$$

where θ_s is the angle along the circumference of the stator, θ_r is the rotor position, θ_e is the flux angle, $P(\theta_s, \theta_r, \theta_e)$ is the permeance function, which is a function of the rotor position and flux angle, $N_x(\theta_s)$ is the winding function for winding x, and $N_y(\theta_s)$ is the winding function for winding y.

Using Fourier series expansions for the permeance and winding functions allows (5) to be evaluated for the harmonics of the permeance and winding functions, relative to the stator angle, that result in nonzero inductance values. For this to occur, the relationship between the harmonics of the permeance and winding functions shown in (6) must be satisfied

$$h_{sp} = h_{sx} + h_{sy} \tag{6a}$$

$$h_{sp} = |h_{sx} - h_{sy}| > 0 \tag{6b}$$

where h_{sp} is the harmonic number of the permeance function as defined by (4), h_{sx} is the harmonic number of the winding function for the x winding, and h_{sy} is the harmonic number of the winding function for the y winding, all relative to the stator angle.

This relationship can be simplified somewhat by realizing that the winding function harmonic numbers, h_{sx} and h_{sy}, by definition, are integer multiples of the number of pole pairs in the machine. This allows the number of pole pairs to be factored out of (6) resulting in the simplified version (7)

$$h_{sp} = m\frac{p}{2} \tag{7}$$

where m is an integer greater than zero and is equal to $2(h_{sx} + h_{sy})/p$ or $2|h_{sx} - h_{sy}|/p$. Note, odd m will not exist if the windings are symmetric, i.e., the winding functions, N_x and N_y, con-

tain only odd harmonics. In this case, (7) is equivalent to the experimentally deduced (4) with n being equal to $m/2$. Equation (7) indicates that the spatial permeance must be periodic over a pole pitch for there to be any coupling between it and the machine windings.

A general relationship between the speed of rotation of the saliencies in a machine and the resulting speed of rotation of the negative-sequence current is much more difficult to calculate in a general manner. This is primarily due to the fact that the exact permeance spatial distribution and variation with changes in flux angle or rotor position is difficult to determine precisely for a given machine. Even with these difficulties, several general statements can be made regarding the characteristics of the speed at which the resulting negative-sequence carrier-signal current rotates.

1) The negative-sequence carrier-signal current will rotate at a speed equal to the spatial harmonic number of the permeance variation, h_{sp}, that it describes times the speed at which this permeance variation rotates. Conceptually this can be seen from the fact that once the permeance variation rotates through an angle equal to its period it appears exactly the same to the machine windings. For example, the main saliency created by saturation has a spatial distribution with a period equal to the pole pitch of the machine and rotates at the same speed that the flux rotates, ω_e. This means that the resulting negative sequence carrier signal current will rotate at twice this speed in electrical units in the negative-sequence carrier-signal reference frame.
2) It is possible for the permeance variation to rotate at a multiple of the speed at which its source rotates. An example of this is the permeance variation caused by the combination of rotor and stator slotting. This permeance variation has a fundamental spatial harmonic given by (8), with S and R being equal to the number of stator and rotor slots, respectively. This permeance waveform rotates at the electrical speed shown in (9), which is a multiple of the speed that its source rotates, i.e., the rotor slotting, which rotates at the rotor mechanical speed ω_{rm} [4], [10]

$$h_{sp} = |R - S| \tag{8}$$

$$\omega_p = \frac{R}{(RS)}\,\omega_{rm}. \tag{9}$$

If the permeance spatial variation due to the stator and rotor slotting couples with the machine windings [h_{sp} is equal to an even integer multiple of the number of pole pairs, (7)] then the resulting negative-sequence carrier-signal current rotates in electrical units equal to the product of (8) and (9).

3) It is possible for negative-sequence carrier-signal current to rotate in the opposite direction that the permeance variation causing it rotates, depending on how the permeance variation couples into the multiphase windings [10]. This coupling with the machine windings is the reason that all of the 4th harmonic (in electrical units) components of the negative-sequence carrier-signal current shown in this paper rotate in the opposite direction that their source rotates, whether they be caused by saturation or the iron bars. In both of these cases the presence of the negative-sequence current can be explained by the coupling between the 1st and 5th harmonics of the stator windings and a permeance variation that is a 4th spatial harmonic of the electrical period (i.e., half a pole pitch) using (6b). The coupling between the two different harmonics of the stator windings causes the resulting inductance variation and negative-sequence current to rotate in the opposite direction that the permeance variation rotates.

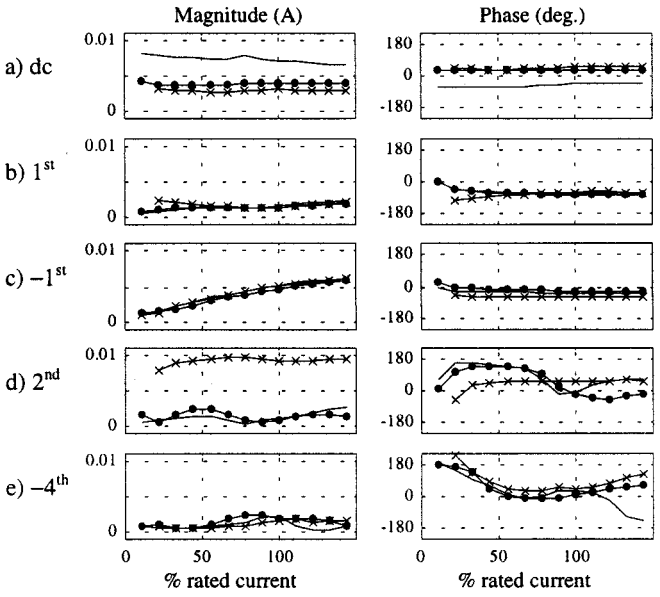

Fig. 15. Magnitude and phase (relative to the fundamental current complex vector) of the most significant fundamental excitation-dependent negative-sequence harmonics as a function of the fundamental current level, for the case of no rotor (• line, $\omega_e = 2$ Hz), no load [x line, $\omega_e = \omega_r = 2$ Hz (60 r/min)], and locked rotor (continuous line, $\omega_e = 2$ Hz).

V. Decoupling of Saturation-Induced Saliencies

The results of this work have shown that saturation due to the stator leakage flux is the source for a majority of the saturation-induced saliencies observed. This is advantageous since the positions of such saliencies are related to the known stator current complex vector.

Fig. 15 shows the variation, both in magnitude and phase, of the most significant harmonics for the test motor 1 (Table I), as a function of the fundamental current level for the cases of no rotor, no load, and rotor locked. It is noted that for the case of locked rotor experiments, the rotor saliency is stationary and dominates the stationary saliency seen in Fig. 15(a). For the case of no-load experiments, the rotor rotates at the same speed as the fundamental excitation and the rotor saliency dominates the 2nd harmonic component. Though not included in this paper, similar harmonic distributions were found for other machines from different manufacturers with similar power ratings as this motor. For the machines tested it appeared that the harmonic distribution depends on the machine ratings. In the machines tested, the $\pm\omega_e$ harmonics were found to decrease as the machine power increased.

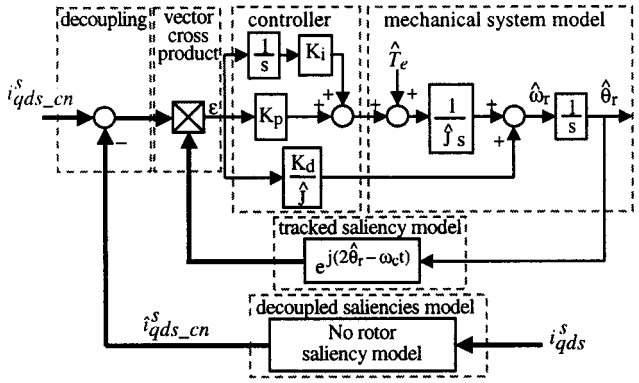

Fig. 16. Tracking observer for estimating rotor position in a machine with a single-rotor position-dependent saliency with negative-sequence carrier signal decoupling based on measurements with the rotor removed, implemented in a stationary reference frame.

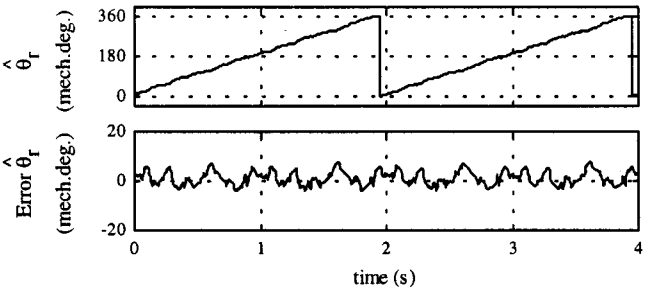

Fig. 17. Estimated rotor position and estimated rotor position error, with $\omega_e = 1$ Hz, $\omega_r = 1$ Hz (30 r/min), and rated flux, with 1st, -1st, 2nd, and -4th harmonics decoupled according to Fig. 15.

An important characteristic observed in these curves is that the variations of the different harmonics are smooth functions. This makes lookup tables viable for storing how the negative-sequence current harmonics vary as a function of the fundamental current, allowing their effects to be decoupled. In addition, only small variations appear to exist for any of the depicted harmonics between the three working conditions considered, i.e., no load, rotor locked (at rated slip), and no rotor, other than the aforementioned influence of the rotor slotting saliency. This suggests using the harmonics measured from the no-rotor experiment to decouple the harmonics created during the normal operation of the motor. These measurements can easily be made on a new machine designed for sensorless applications. On the other hand, collecting this data from currently installed machines might be impractical due to the necessary downtime and the excessive effort required. For these situations, useful data can also be collected from locked-rotor and no-load experiments. In any case, the decoupling of saturation-induced saliencies necessarily requires a commissioning process.

Fig. 16 shows the decoupling scheme used, and Fig. 17 the estimated position under a rated-flux, no-load condition, after decoupling the four most significant saturation-induced harmonics, i.e., the 1st, -1st, 2nd, and -4th .

The "no-rotor saliency model" block implements the measured data shown in Fig. 15 for the case of the rotor removed using a lookup table. This block provides an estimate of the negative-sequence carrier current due to stator leakage flux saturation. Comparing Fig. 17 with Fig. 10, a noticeable improvement in the estimated position is seen.

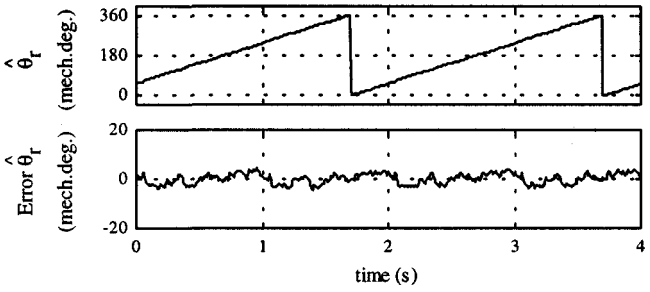

Fig. 18. Estimated rotor position and estimated rotor position error, with rated current at rated slip, $\omega_e = -1$ Hz, $\omega_r = 1$ Hz (30 rmin), with 1st, -1st, 2nd, and -4th harmonics decoupled according to Fig. 15.

Fig. 18 shows the estimated position under rated flux, rated slip, i.e., rated fundamental current, after decoupling the four most significant harmonics in a similar way as was done for Fig. 17. The improvement in estimated position can again be observed when comparing Fig. 18 with Fig. 8.

VI. Conclusions

The influence of saturation-induced saliencies on the performance of carrier-signal injection-based sensorless ac drives has been studied in this paper.

While saturation-induced saliencies can be due to air-gap, stator leakage, and rotor leakage flux, an important portion of the overall saturation-induced saliencies has been shown to be a function of the stator leakage flux. The locations of these saliencies are governed by the stator current vector, which is well known both in magnitude and phase.

A lookup table experimentally measured with the rotor removed was found to yield a very useful approximation to these stator leakage flux saliencies. These "no-rotor" data were shown to be valid over the full range of drive operation.

The lookup table containing the most relevant harmonics of the negative-sequence carrier-signal current relative to the location of the fundamental stator current was shown to be a viable means of decoupling errors due to the stator leakage saturation-induced saliencies.

References

[1] P. L. Jansen and R. D. Lorenz, "Transducerless position and velocity estimation in induction and salient AC machines," *IEEE Trans. Ind. Applicat.*, vol. 31, pp. 240–247, Mar./Apr. 1995.

[2] ——, "Transducerless field orientation concepts employing saturation-induced saliencies in induction machines," *IEEE Trans. Ind. Applicat.*, vol. 32, pp. 1380–1393, Nov./Dec. 1996.

[3] M. Corley and R. D. Lorenz, "Rotor position and velocity estimation for a permanent magnet synchronous machine at standstill and high speeds," *IEEE Trans. Ind. Applicat.*, vol. 35, pp. 784–789, July/Aug. 1999.

[4] M. W. Degner and R. D. Lorenz, "Position estimation in induction machines utilizing rotor bar slot harmonics and carrier frequency signal injection," *IEEE Trans. Ind. Applicat.*, vol. 36, pp. 736–742, May/June 2000.

[5] J. Ha and S. K. Sul, "Sensorless field orientation control of an induction machine by high frequency signal injection," *IEEE Trans. Ind. Applicat.*, vol. 35, pp. 45–51, Jan./Feb. 1999.

[6] M. W. Degner and R. D. Lorenz, "Using multiple saliencies for the estimation of flux, position, and velocity in AC machines," *IEEE Trans. Ind. Applicat.*, vol. 34, pp. 1097–1104, Sept./Oct. 1998.

[7] L. A. S. Ribeiro, M. W. Degner, F. Briz, and R. D. Lorenz, "Comparing carrier frequency voltage and current injection for the estimation of flux, position and velocity in sensorless AC drives," in *Conf. Rec. IEEE-IAS Annu. Meeting*, St. Louis, MO, Oct. 1998, pp. 452–459.
[8] J. Cilia, G. M. Asher, and K. G. Bradley, "Sensorless position detection for vector controlled induction motor drives using an asymmetric outer-section cage," in *Conf. Rec. IEEE-IAS Annu. Meeting*, San Diego, CA, Oct. 1996, pp. 286–292.
[9] P. L. Jansen, "The integration of state estimation, control, and design for induction machines," Ph.D. dissertation, Dept. Elect. Comput. Eng., University of Wisconsin, Madison, 1993.
[10] M. W. Degner, "Flux, position and velocity estimation in AC machines using carrier frequency signal injection," Ph.D. dissertation, Dept. Elect. Comput. Eng., University of Wisconsin, Madison, 1998.
[11] N. Teske, G. M. Asher, K. J. Bradley, and M. Sumner, "Sensorless position control of induction machines using rotor saliencies under load conditions," in *Proc. EPE'99*, Lausanne, Switzerland, 1999, CD-ROM.
[12] F. Briz, A. Diez, and M. W. Degner, "Dynamic operation of carrier signal injection based, sensorless, direct field oriented AC drives," *IEEE Trans. Ind. Applicat.*, vol. 36, pp. 1360–1368, Sept./Oct. 2000.
[13] M. L. Aime, M. W. Degner, and R. D. Lorenz, "Saturation measurements in AC machines using carrier signal injection," in *Conf. Rec. IEEE-IAS Annu. Meeting*, St. Louis, MO, Oct. 1998, pp. 159–166.
[14] A. Consoli, G. Scarcella, and A. Testa, "A new zero frequency flux position detection approach for direct field oriented control drives," *IEEE Trans. Ind. Applicat.*, vol. 36, pp. 797–804, May/June 2000.
[15] S. W. Smith, *The Scientist and Engineer's Guide to Digital Signal Processing*. San Diego, CA: California Technical, 1997.
[16] P. L. Alger, *Induction Machines—Their Behavior and Uses*, 2nd ed. New York: Gordon and Breach, 1970.

Fernando Briz received the M.S. and Ph.D. degrees from the University of Oviedo, Gijón, Spain, in 1990 and 1996, respectively.

From June 1996 to March 1997, he was a Visiting Researcher at the University of Wisconsin, Madison. He is currently an Associate Professor in the Electrical Engineering Department, University of Oviedo. His topics of interest include control systems, high-performance ac drives control, sensorless control, and digital signal processing.

Prof. Briz received a Prize Paper Award from the Industrial Power Converter Committee of the IEEE Industry Applications Society.

Michael W. Degner (S'95–A'98–M'99) received the B.S., M.S., and Ph.D. degrees in mechanical engineering from the University of Wisconsin, Madison, in 1991, 1993, and 1998, respectively, with a focus on electric machines, power electronics, and control systems.

He is currently with the Scientific Research Laboratory, Ford Motor Company, Dearborn, MI, where his research is focused on the use of power electronics in automobile applications. His interests include control systems, machine drives, electric machines, power electronics, and mechatronics.

Alberto Diez received the M.S. and Ph.D. degrees from the University of Oviedo, Gijón, Spain, in 1983 and 1988, respectively.

He is currently an Associate Professor in the Electrical Engineering Department, University of Oviedo. In October 1998, he was nominated as a Member of the Executive Committee D2 "Rolling-flat products" by the European Commission. His topics of interest include control systems, high-performance ac drives control, and industrial automation processes.

Robert D. Lorenz (S'83–M'84–SM'91–F'98) received the B.S., M.S., and Ph.D. degrees from the University of Wisconsin, Madison, and the M.B.A. degree from the University of Rochester, Rochester, NY.

Since 1984, he has been a member of the faculty of the University of Wisconsin, Madison, where he is the Consolidated Papers Foundation Professor of Controls Engineering in both the Mechanical Engineering and Electrical and Computer Engineering Departments. He is Co-Director of the Wisconsin Electric Machines and Power Electronics Consortium. He is also the thrust leader for control and sensor integration in the Center for Power Electronic Systems, an NSF Engineering Research Center which is a joint ERC with Virgina Polytechnic Institute and State University, Rensselaer Polytechnic Institute, University of Puerto Rico-Mayaguez, and North Carolina A&T. From 1972 to 1982, he was a member of the research staff at the Gleason Works, Rochester, NY, working principally on high-performance drives and synchronized motion control. He was a Visiting Research Professor in the Electrical Drives Group, Catholic University of Leuven, Leuven, Belgium, in the summer of 1989 and at the Power Electronics and Electrical Drives Institute, Technical University of Aachen, Aachen, Germany, in the summers of 1987, 1991, 1995, 1997, and 1999, where he was also the SEW Eurodrive Guest Professor until June 30, 2001. In 1969–1970, he conducted Master thesis research at the Technical University of Aachen. His current research interests include sensorless electromagnetic motor/actuator technologies, real-time signal processing and estimation techniques, precision multiaxis motion control, and ac drive and high-precision machine control technologies.

Dr. Lorenz is the IEEE Industry Applications Society (IAS) President for 2001, a Distinguished Lecturer of the IAS for 2000/2001, the immediate past Chair of the IAS Awards Department, past Chairman of the IAS Industrial Drives Committee, and a member of the IAS Industrial Drives, IAS Electric Machines, IAS Industrial Power Converter, and IAS Industrial Automation and Control Committeess. He is a member of the IEEE Sensor Council AdCom and the IEEE Neural Network AdCom. He is a Registered Professional Engineer in the States of New York and Wisconsin. He is also a member of the American Society of Mechanical Engineers, Instrument Society of America, and Society of Photo-Optical Instrumentation Engineers.